Computational Thermal Sciences, 8 (3): 291–308 (2016)

FLOW AND HEAT TRANSFER SIMULATION OF THREE DIFFERENT NANOFLUIDS IN A CAVITY WITH SINUSOIDAL BOUNDARY CONDITIONS UNDER THE INFLUENCE OF AN INCLINED MAGNETIC FIELD USING LBM: A PHASE DEVIATION APPROACH

Amir Javad Ahrar & Mohammad Hassan Djavareshkian*

Ferdowsi University of Mashhad, Iran

*Address all correspondence to: Associate Professor Mohammad Hassan Djavareshkian,
E-mail: javareshkian@um.ac.ir

In the present study, a nanofluid–filled cavity with sinusoidal temperature boundary condition under the influence of an inclined magnetic field was investigated numerically. The lattice Boltzmann method (LBM) was applied to simulate the nanofluid flow with water as the carrier fluid and for three different nanoparticle types: Al_2O_3, Cu, and TiO_2. More than 1100 individual tests were carried out in this work to show the combined effect of the nanoparticles and magnetic field situations. It goes without saying that nanoparticles are meant to improve the heat transfer rate, because unlike the magnetic field they are not present in any system on their own, but they're added manually to enhance the Nusselt number. However, it is seen that in some magnetic situations (field intensity and direction) adding the volume fraction of nanoparticles cannot help the heat transfer increment. The flow and heat transfer behavior of these three nanofluids were observed for different Rayleigh numbers (10^3–10^6), Hartmann numbers (0–80), nanoparticle volume fraction (0–6%), magnetic field direction θ = 0–90°, and temperature boundary condition phase deviation γ = 0–90°. The results indicated that the influence of nanoparticles for this geometry and boundary conditions is highly dependent on the Rayleigh and Hartmann numbers. Although the magnetic field direction plays an unimportant role in lower Rayleigh numbers, the effects will become most significant for moderate Rayleigh numbers like 10^5.

KEY WORDS: *magneto-hydro-dynamics, nanoparticle volume fraction, magnetic field intensity and direction*

1. INTRODUCTION

Generally, cavities can be classified into two major groups: closed and open cavities. The classical problem of natural convection in closed cavities has been investigated widely due to its significant applications in many industries such as: solar concentrators, lakes and reservoirs, refrigeration, the cooling process of electric devices, and fire research (Abu-Mulaweh, 2003; Clausing, 1983). Also, there has been an increasing interest in studying the flow behavior and heat transfer mechanism of cavities under the influence of a magnetic field, and many different solution techniques, working situations, and boundary conditions have been considered in the open literature so far. The wide occurrence of magneto-hydro-dynamics (MHD) in many industrial cases, e.g., crystal growth, metal casting, fusion reactors, and geothermal energy extractions, make it undeniable (Ahrar et al., 1995; Ozoe and Okada, 1989).

Al-Nimr (1995) obtained analytical solutions for MHD fully developed upward (heating) or downward (cooling) natural convection in open–ended porous annuli. Later on, Al-Nimr and Hader (1999) modified their solution for more general thermal boundary conditions. Ishikawa et al. (2000) numerically investigated the natural convection with density inversion in a square cavity with variable fluid properties. Hossain and Rees (2005) studied unsteady laminar

1940–2503/16/$35.00

NOMENCLATURE

B	magnetic field
C_p	specific heat at constant pressure
c_i	discrete particle speeds
c	lattice speed
F	external forces
f	density distribution functions
f^{eq}	equilibrium density distribution functions
g	internal energy distribution functions
g^{eq}	equilibrium internal energy distribution functions
g_y	gravity
Ha	Hartmann number
M	lattice number in y direction
Ma	Mach number
Nu	Nusselt number
Pr	Prandtl number
Ra	Rayleigh number
T	temperature
x, y	Cartesian coordinates
u, v	velocity components in x and y direction

Greek Symbols

α	thermal diffusivity
β	thermal expansion coefficient
γ	phase deviation
θ	inclination angle of magnetic field
μ	dynamic viscosity
ν	kinematic viscosity
ρ	density
τ_ν	relaxation time for flow
σ	electrical conductivity
τ_α	relaxation time for temperature
φ	volume fraction
ω_i	weighted factor in i direction

Subscripts

c	cold
f	fluid
H	hot
nf	nanofluid
s	nanoparticles

natural convection of water in a rectangular cavity and found that the heat generation rate and the mean temperature of solid walls play an important role in the flow and temperature fields.

Kandaswamy et al. (2008) investigated the heat transfer rate of partially active walls of a square cavity. They found that the heat transfer rate is maximum for middle-middle thermally active locations and it is very poor for the top-bottom locations. Also, Sivasankaran et al. (2011) numerically investigated the magneto-convection of cold water in an open cavity with variable fluid properties. In their work it was observed that the convection heat transfer is enhanced by thermo-capillary force when buoyancy force is weakened. Oztop et al. (2011) made a numerical study on the MHD mixed convection in a lid–driven cavity with a corner heater. They applied a finite-volume technique to observe the fluid flow and temperature fields under different Grashof and Hartmann numbers. They have taken the Joule effect under account in their study. Ahrar and Djavareshkian (2014) used the lattice Boltzmann method (LBM) to simulate the MHD convection of air in a lid-driven cavity with heated walls. They studied the influence of Hartmann number and magnetic field direction on the convection heat transfer rate.

By and by, nano- and micro-fluids have been brought into light by researchers in the MHD field. Not only because of their outstanding function in heat dissipation but also for their flow control behaviors under a magnetic field (e.g., ferrofluids), they soon became very popular (Shahrul et al., 2014). Analytical solutions were not available for complicated geometries and experimental study of nanofluids always had their own difficulties, so the attempts to simulate their flow and heat transfer numerically were accelerated in recent years (Ahmed et al., 2015; Minakov et al., 2015).

Khanafer et al. (2003) tried to simulate numerically the flow and heat transfer of Cu-water nanofluid using the finite–volume (FV) approach. In their work, four different methods for nanofluid treatment were examined and the results were compared to the experimental data. In 2011, Ghasemi et al. (2011) also used FV method to investigate the Al_2O_3–water nanofluid flow characteristics under the influence of a magnetic field source. They proclaimed that the heat transfer rate increases with an increase of the Rayleigh number but it decreases with the increment of Hartmann number. They also reported that for certain Ha and Ra numbers there could be situations where adding Al_2O_3 nanoparticles would decrease the Nu number.

The kinetic nature and the simple usage of LBM, along with its exact and accurate solutions, made it a promising tool in simulation of nanofluids. Nemati et al. (2012) used this method to study the magnetic field effects on natural convection flow of different nanofluids in a rectangular cavity. They found that the average Nusselt number increases for nanofluid when increasing the solid volume fraction, while in the presence of a strong magnetic field, this effect decreases. In 2014, Kefayati used LBM to analyze the heat dissipation of ferrofluids in a linearly heated cavity. He used an external magnetic field source on a flow regime of Ra = 10^3–10^5 for a cobalt nanoparticle volume fraction between 0 and 3% in kerosene. Unlike many others, he reported that the heat transfer decreases by the increment of the particle volume fraction. It seemed that using a non-uniform temperature boundary condition in addition to MHD forces can change the heat transfer effect of nanoparticles. In the same year, Mahmoudi et al. (2014), in an independent effort, tried to investigate Al_2O_3–water flow in an enclosure with linearly heated walls. They examined the fluid flow under the influence of a magnetic field with changing the field direction. They presented the results for different Ha and magnetic field angles. In their work, there is no doubt that there are a few magnetic situations in which adding nano-particles will decrease the average Nu number of the surface.

It goes without saying that non-uniform temperature boundary conditions such as partially heating walls (Gangawane et al., 2015; Hussein et al., 2014) and linear (Kefayati et al., 2012) or sinusoidal (Kefayati, 2015; Wu et al., 2015) temperature boundary conditions are of most interest in the closed cavities. So in this paper we tried to simulatethese three types of nanofluid flow in a cavity with sinusoidal temperature walls boundary conditions for a wide range of Ha (0–80) and for magnetic field angles θ = 0–90° and phase deviation of γ = 0–90°. Evidently, a Cu nanoparticle with K_s = 400 is considered as one of the best nanoparticles for heat transfer (Ahrar and Djavareshkian, 2016), Al_2O_3 has a moderate thermal conductivity of 40, and TiO_2 has a low thermal conductivity of about 9. So in order to increase the heat transfer rate, in the present work these three different nanoparticles are chosen to compare the enhancing effect of adding nanoparticles to the fluid versus changing the magnetic field intensity and direction, for this specific boundary condition.

2. PROBLEM STATEMENT AND FORMULATION

2.1 The Classical Form of Formulation

The continuity, momentum, and energy equations (1)–(4) for nanofluid MHD flow in dimensional form can be written as follows:

$$\frac{\delta u}{\delta x} + \frac{\delta \nu}{\delta y} = 0 \tag{1}$$

$$\rho_{nf}\left(u\frac{\delta u}{\delta x} + \nu\frac{\delta \nu}{\delta y}\right) = -\frac{\delta P}{\delta x} + \mu_{nf}\left(\frac{\delta^2 u}{\delta x^2} + \frac{\delta^2 \nu}{\delta y^2}\right) + F_x \tag{2}$$

$$\rho_{nf}\left(u\frac{\delta \nu}{\delta x} + \nu\frac{\delta \nu}{\delta y}\right) = -\frac{\delta P}{\delta y} + \mu_{nf}\left(\frac{\delta^2 \nu}{\delta x^2} + \frac{\delta^2 \nu}{\delta y^2}\right) + F_y \tag{3}$$

$$u\frac{\delta T}{\delta x} + \nu\frac{\delta T}{\delta y} = \alpha_{nf}\left(\frac{\delta^2 T}{\delta x^2} + \frac{\delta^2 T}{\delta y^2}\right) \tag{4}$$

where F_x and F_y are the total body forces in x and y directions, respectively, and can be defined as

$$F_x = \frac{\mathrm{Ha}^2 \mu_{nf}}{L^2}(\nu \sin\theta\cos\theta - u\sin^2\theta) \tag{5}$$

$$F_y = \frac{\mathrm{Ha}^2 \mu_{nf}}{L^2}(u \sin\theta\cos\theta - \nu\cos^2\theta) + \rho_{nf} g_y \beta_{nf}(T - T_c) \tag{6}$$

In the above equations, Ha = $LB\sqrt{\sigma_{nf}/\mu_{nf}}$ is the Hartmann number, where σ is electrical conductivity, B is the magnitude of the magnetic field, L is the length of the cavity, and θ is the direction of the magnetic field.

2.2 Simulation of MHD with the Lattice Boltzmann Method

2.2.1 Brief Introduction to LBM

The LBM method with a standard two–dimensional, nine–velocity (D2Q9) system for both temperature and flow field is applied in this study. For the sake of completeness, a brief review of the lattice Boltzmann method is included. The discretized LBM equations with external force in nine directions can be written as follows:

$$f_i(x + c_i\Delta t, t + \Delta t) - f_i(x,t) = -\frac{1}{\tau_\nu}\left[f_i(x,t) - f_i^{eq}(x,t)\right] + \Delta t F \tag{7}$$

$$g_i(x + c_i\Delta t, t + \Delta t) - g_i(x,t) = -\frac{1}{\tau_\nu}\left[g_i(x,t) - g_i^{eq}(x,t)\right] \tag{8}$$

Equations (7) and (8) are used to solve the flow and temperature fields, respectively. Equation (7) recovers the continuity and momentum equations (1–3), where the total body forces were considered by the external force of Eq. (7). Equation (8) describes the evaluation of the internal energy and leads to Eq. (4). In the above equations f_i^{eq} and g_i^{eq} are the equilibrium distribution functions for flow and temperature field, respectively, and can be calculated as follows:

$$f_i^{eq} = \omega_i \rho \left[1 + \frac{c_i u}{c_s^2} + \frac{1}{2}\frac{(c_i u)^2}{c_s^4} - \frac{1}{2}\frac{uu}{c_s^2}\right] \tag{9}$$

$$g_i^{eq} = \omega_i T \left[1 + \frac{c_i u}{c_s^2} + \frac{1}{2}\frac{(c_i u)^2}{c_s^4} - \frac{1}{2}\frac{uu}{c_s^2}\right] \tag{10}$$

where c_s is the lattice speed of sound, which is equal to $c_s = c/\sqrt{3}$, and the discrete velocities c_i for D2Q9 are also defined as

$$c_i = \begin{cases} 0 & \text{for} \quad i = 0 \\ c\left[\cos\left(\dfrac{i\pi}{2} - \dfrac{\pi}{2}\right),\ \sin\left(\dfrac{i\pi}{2} - \dfrac{\pi}{2}\right)\right] & \text{for} \quad i = 1-4 \\ c\sqrt{2}\left[\cos\left(\dfrac{i\pi}{2} - \dfrac{9\pi}{4}\right),\ \sin\left(\dfrac{i\pi}{2} - \dfrac{9\pi}{4}\right)\right] & \text{for} \quad i = 5-8 \end{cases} \tag{11}$$

In the above equations c is equal to $\Delta x/\Delta t$, with Δx and Δt being the lattice space and lattice time step, respectively. The weighing factors for the D2Q9 model are obtained as

$$\omega_i = \begin{cases} \dfrac{4}{9} & \text{for} \quad i = 0 \\ \dfrac{1}{9} & \text{for} \quad i = 1-4 \\ \dfrac{1}{36} & \text{for} \quad i = 5-8 \end{cases} \tag{12}$$

The kinematic viscosity ν and the thermal diffusivity α are then related to the relaxation times by Eqs. (13) and (14):

$$\nu = \left[\tau_\nu - \frac{1}{2}\right] c_s^2 \Delta t \tag{13}$$

$$\alpha = \left[\tau_\alpha - \frac{1}{2}\right] c_s^2 \Delta t \tag{14}$$

2.2.2 Applying Body Forces in LBM

In order to apply the effect of magnetic field and gravitational forces (body forces), a force term F was added to the density distribution function equations. To obtain F all variables must become dimensionless with the lattice units. So the external force appears for LBM as follows:

$$F = F_x + F_y \tag{15}$$

$$F_i = \omega_i F c_i / c_s^2 \tag{16}$$

$$F_{ix} = 3\omega_i \rho \left[\frac{\mathrm{Ha}^2 \nu}{M^2} (\nu \sin\theta \cos\theta - u \sin^2\theta) \right] \tag{17}$$

$$F_{iy} = 3\omega_i \rho \left[[g_y \beta (T - T_c)] + \frac{\mathrm{Ha}^2 \nu}{M^2} (u \sin\theta \cos\theta - \nu \sin^2\theta) \right] \tag{18}$$

In the above equations M is the number of lattices in the specific length L direction, and the total body force term F can be produced from the summation of (17) and (18).

2.2.3 Nondimensional Parameters

For fixed Rayleigh, Mach, and Prandtl numbers, the kinematic viscosity can be calculated from the following equation:

$$\nu_f = M \,\mathrm{Ma}\, c_s \sqrt{\frac{\mathrm{Pr}}{\mathrm{Ra}}} \tag{19}$$

Also, the thermal diffusivity can be defined from the Prandtl number as

$$\mathrm{Pr} = \frac{\nu_f}{\alpha_f} \tag{20}$$

In the above correlations the Rayleigh number is defined as Ra = $g_y \beta_f M^3 (T_h - T_c)/\nu_f \alpha_f$, with $T_h = 1$ and $T_c = 0$, and in order to avoid any compressibility errors, the Ma number is kept at 0.1. Evidently, the Nusselt number is one of the most important dimensionless parameters in the description of the convective heat transfer. In this paper, the local Nusselt number of each wall, the average Nu on the heating part of both walls, $\mathrm{Nu}^*(\varphi)$ and $\widehat{\mathrm{Nu}}(\mathrm{Ha}, \theta)$ are calculated from the following equations:

$$\mathrm{Nu}(y) = -\frac{K_{nf}}{K_f} \frac{M}{T_h - T_c} \frac{\delta T}{\delta n} \tag{21}$$

$$\widehat{\mathrm{Nu}} = \frac{1}{H} \int_{Heating\ half} \mathrm{Nu}_{leftwall} dy + \frac{1}{H} \int_{Heating\ half} \mathrm{Nu}_{right\ wall} dy \tag{22}$$

$$\mathrm{Nu}^*(\varphi) = \frac{\overline{\mathrm{Nu}}(\varphi)}{\overline{\mathrm{Nu}}(\varphi = 0)} \tag{23}$$

$$\widehat{\mathrm{Nu}}(\mathrm{Ha}, \theta) = \frac{\overline{\mathrm{Nu}}(\mathrm{Ha}, \theta)}{\overline{\mathrm{Nu}}(\mathrm{Ha} = 0)} \tag{24}$$

Here, $\mathrm{Nu}^*(\varphi)$ refers to the ratio of the average Nu with the nanoparticles volume fraction of φ to the average Nu number of the pure fluid.

2.3 Modeling of Nanofluid

In this simulation, the dynamical similarity depends on the dimensionless parameters of Rayleigh number Ra, Prandtl number Pr, and Hartmann number Ha. Due to the assumption of the nanofluid as a pure fluid, the mixture qualities are to be calculated and applied in these dimensionless parameters. The thermo-physical properties of the nanofluid are fixed during the iteration process, except for the density, which is obtained from the Boussinesq assumption.

The density (ρ), the specific heat (C_p), and the thermal expansion coefficient (β) of the nanofluid are calculated as follows:

$$\rho_{nf} = (1-\varphi)\rho_f + \varphi\rho_s \tag{25}$$

$$(\rho C_p)_{nf} = (1-\varphi)(\rho C_p)_f + \varphi(\rho C_p)_s \tag{26}$$

$$(\rho\beta)_{nf} = (1-\varphi)(\rho\beta)_f + \varphi(\rho\beta)_s \tag{27}$$

Also, according to the Brinkman model, the viscosity of a mixture containing a dilute suspension of small rigid spherical particles can be obtained from

$$\mu_{nf} = \frac{\mu_f}{(1-\varphi)^{2.5}} \tag{28}$$

and the effective thermal conductivity of the mixture can be approximated by the Maxwell-Garnetts (MG) model as

$$\frac{K_{nf}}{K_f} = \frac{K_s + 2K_f + 2(K_f - K_s)}{K_s + 2K_f - \varphi(K_f - K_s)} \tag{29}$$

Also it is worth mentioning that the MG model is restricted only to spherical nanoparticles and does not take into account the shape of nanoparticles. Finally, the electrical conductivity σ of the nanofluid is calculated from the Maxwell model (Sheikholeslami et al., 2012):

$$\sigma_{nf}/\sigma_f = \frac{1 + 3\varphi\,(\sigma_s/\sigma_f - 1)}{(\sigma_s/\sigma_f + 2) - 2\varphi\,(\sigma_s/\sigma_f - 1)} \tag{30}$$

with φ being the solid volume fraction and subscripts nf, f, and s referring to the nanofluid, carrier fluid, and the nanoparticles, respectively. The thermophysical properties of water and the nanoparticles are presented in Table 1.

3. NUMERICAL APPROACH AND VALIDATION

3.1 Geometry and Boundary Conditions

Figure 1 shows a schematic outline of the enclosure filled with Cu-water nanofluid. The cavity is bounded with two adiabatic walls (south and north) and two sinusoidal varying temperature walls (west and east). The temperature distribution for the west wall is $T(y) = T_c + \sin(2\pi y/H)$ and the phase deviation with the east wall is equal to γ. In this study, it is assumed that the nanofluid is Newtonian, the induced magnetic field produced by the motion of

TABLE 1: Thermophysical properties of nanoparticles (NPs) and the carrier fluid

	μ (kg/ms)	ρ (kg/m^3)	C_p (J/kg K)	K (W/mK)	β (1/K)$\times 10^{-5}$	σ (ω m)$^{-1}$
Pure water	0.00089	997.1	4179	0.613	21	0.05
Al_2O_3 NPs	—	3970	765	40	0.85	596×10^5
Cu NPs	—	8954	383	400	1.67	596×10^5
TiO_2 NPs	—	4250	686.2	8.9538	0.9	596×10^5

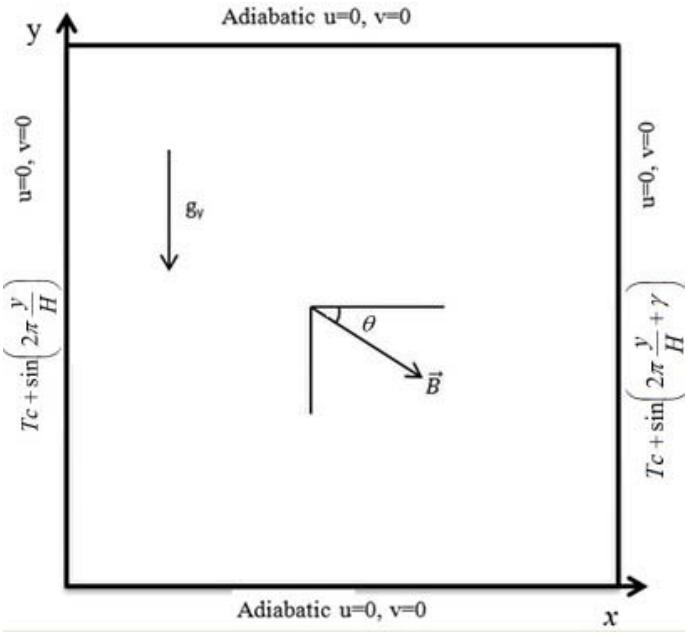

FIG. 1: The schematic outline of the geometry including the boundary conditions

an electrically conducting fluid is negligible compared to the applied magnetic field, and the nanoparticles are in thermal equilibrium with water and they flow with the same velocity, while there is no slip between the base fluid and the nanoparticles. The flow regime is also considered to be steady, two dimensional, incompressible, and laminar. Moreover, the effects of Joule heating, viscous dissipation, and radiation heat transfer are neglected in the current study.

3.2 Code Validation and Mesh Independance

In the present study, an in-house SRT (i.e., single relaxation time) lattice Boltzmann code was developed in FORTRAN to simulate the flow and temperature fields in the mentioned cavity. The numerical results were validated with four different published data. First the boundary conditions and the natural convection with Bossinesq assumption were tested against the study of Deng and Chang (2008) for Ra = 10^5, Pr = 0.7. The results for the streamlines and isotherms are shown in Fig. 2. Then the reliability of the code in simulation of nanofluids flow was investigated. The predicted data for Gr = 10^5 and φ = 10% for a uniform temperature boundary condition with Cu nanoparticles were compared to the results of Khanafer et al. (2003) and Jahanshahi et al. (2010).

Figure 3 presents the dimensionless temperature distribution along the horizontal middle section line of the cavity. Afterward, in order to show the accuracy of the simulations under the influence of a magnetic field, the average Nusselt numbers of the present study and Ghasemi et al. (2011) at Ra = 10^5, for three different Ha numbers of 0, 30, and 60, and volume fractions of 0, 4, and 6%, are listed in Table 2. The nanoparticles of this case are Al_2O_3 and the boundary conditions are uniform temperature boundary conditions again. The results in all cases showed a perfect match and proved this developed code to be a quality tool in the simulations of MHD natural convection for nanofluids. Also, to show the simulations are mesh independent, the results of the average Nusselt number for the highest Hartmann number (Ha = 90) in this study and for Ra = 10^5, 10^6 are presented in Fig. 4 for six different meshes of 20×20, 40×40, 60×60, 80×80, 100×100, 120×120. As can be seen, there is a negligible difference between the results of the meshes of 100×100 and 120×120, so in this study a 100×100 mesh was chosen for the rest of the simulation.

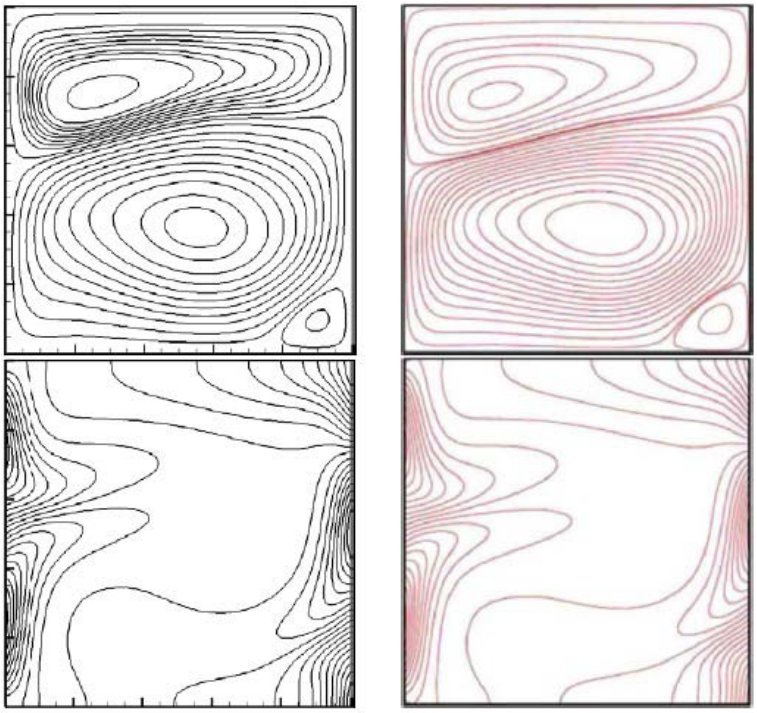

FIG. 2: The streamlines and isotherms for the present study **(left)** and Deng and Chang (2008) **(right)** for Ra = 10^5 and Pr = 0.7

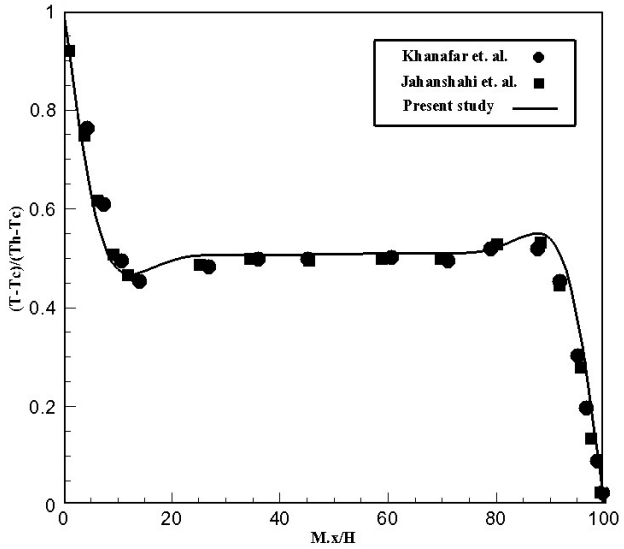

FIG. 3: Validation of the results for nanofluid flow at Gr = 10^5, Pr = 6.2, and φ = 10% for the present study and Khanafer et al. (2003) and Jahanshahi et al. (2010)

4. RESULTS AND DISCUSSION

Figures 5 and 6 represent the streamlines and isotherms in the cavity for the flow at Ra = 10^5 and Ha = 40. In this simulation, various magnetic field directions (θ) and temperature boundary condition phase deviations of west and

TABLE 2: Comparison of the results of $\overline{Nu}$ for the present study and Ghasemi et al. (2011)

	φ = 0 (Present study)	φ = 0 (Ghasemy et al.)	Error %	φ = 0.04 (Present study)	φ = 0.04 (Ghasemy et al.)	Error %	φ = 0.06 (Present study)	φ = 0.06 (Ghasemy et al.)	Error %
Ha = 0	4.721503	4.738	0.348	4.88497	4.896	0.225	4.959111	4.968	0.178
Ha = 30	3.142508	3.150	0.237	3.111831	3.124	0.389	3.090939	3.108	0.548
Ha = 60	1.864826	1.851	–0.746	1.812983	1.815	0.111	1.796061	1.806	0.550

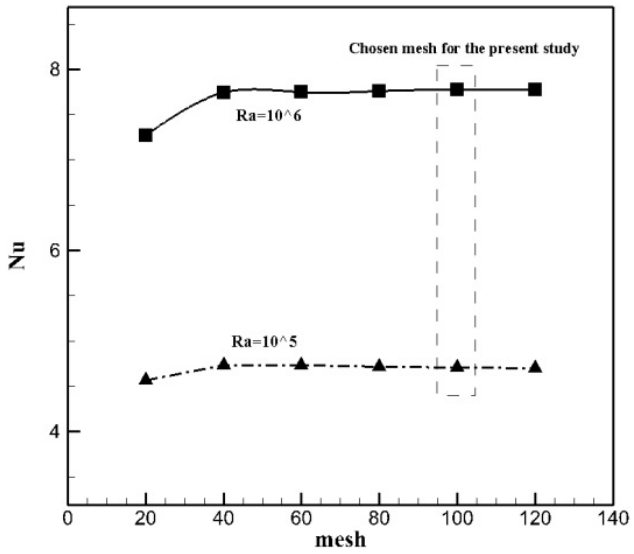

FIG. 4: The results of mesh independence investigation for six uniform meshes

east walls (γ) are applied. It is obvious that the main strong vortex is deformed with a change in the field direction (θ). The magnetic field direction in some cases (especially at $\theta = 90$) can break the main vortex into two weaker vortices. These vortices have lower stream function values and accordingly, they produce lower fluid velocity on the walls. This phenomenon also has a direct influence on the heat transfer rate of the walls, due to the decrease of the convective fluxes. In Fig. 6 one can find that in the cases of stronger vortices, the isotherms produce a much denser profile near the vertical walls, which in this case means a higher temperature derivative and higher Nusselt number on the walls. As can be seen for almost all γs, the isotherms perform denser profiles as θ increases from 0 to 45°, and then the profiles start to expand as we continue increasing the magnetic field angle from 45 to 90°. Also, it is worth mentioning that by increasing the temperature phase deviation from 0 to 90°, the temperature derivative on the vertical walls increases in most of the magnetic field angles. This also can be related to the stronger main vortices for the higher γs.

Figures 7(a)–7(c) demonstrate the local Nusselt for the west (up) and east (down) walls at $Ra = 10^5$ for different Ha numbers, θ angles, and γ values, respectively. In Fig. 7(a) it is obvious that with the Ha increment, the local Nu amplitude decreases at $\theta = 0$, $\gamma = \pi/2$. However, for Hartmann numbers higher than 60°, the change of Nu number is insignificant so it can be concluded that at this Ha, the dominant heat transfer region is changed from convection to conduction heat transfer for this Ra number. Figure 7(b) reveals a slight increase in the Nu(y) with the increment of γ from 0 to 90° on the east wall at Ha = 40, $\theta = 0$, and as was predicted, the highest Nusselt number is observed at $30° \leq \theta \leq 60°$ [Fig. 7(c)].

Figure 8 illustrates the normalized Nu numbers of nanofluids containing a particle volume fraction of $\varphi = 3\%$ with respect to those of the pure fluid (Nu^*) for different Ha numbers of 20, 40, 60, and 80 at $Ra = 10^5$ versus magnetic

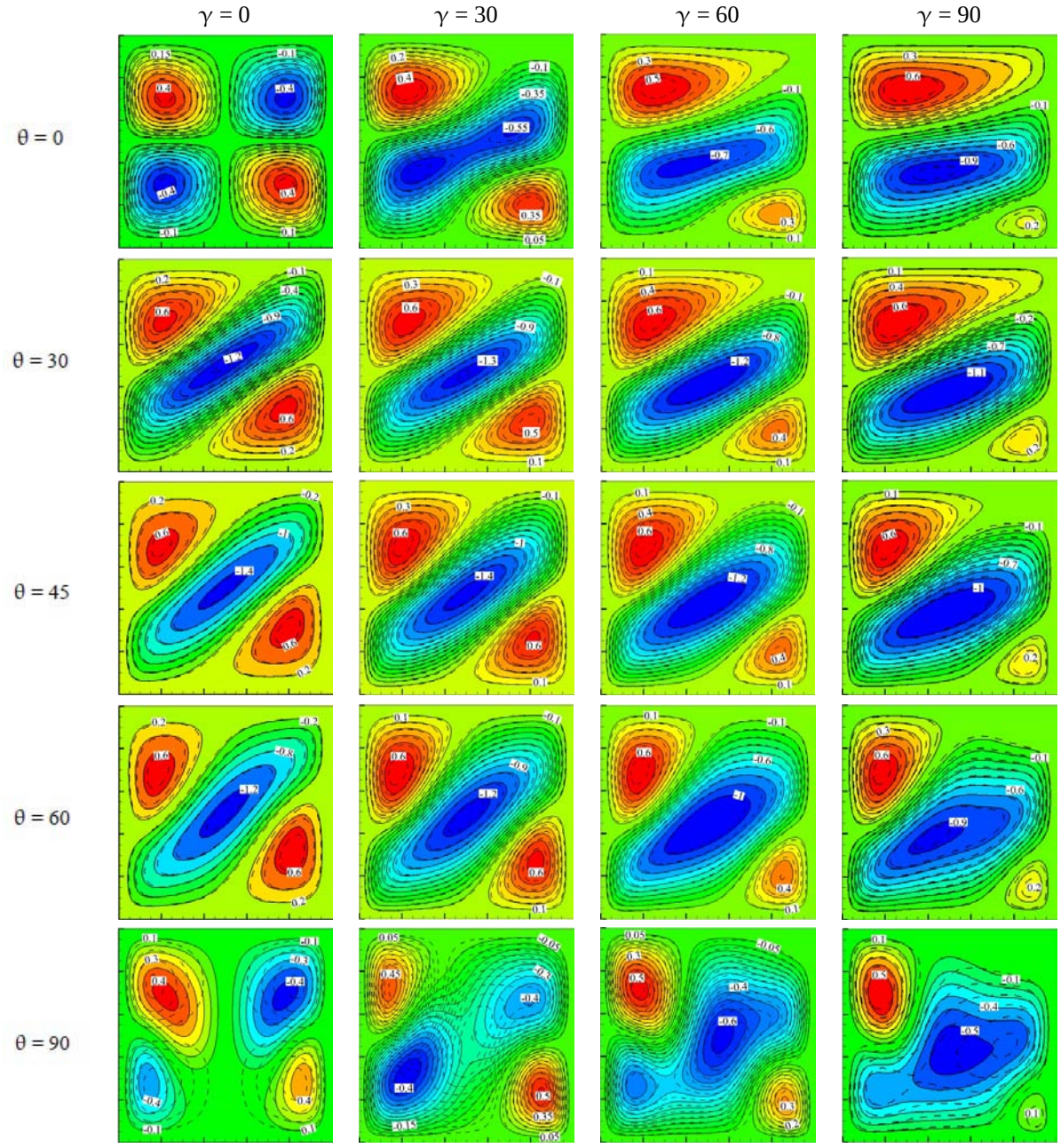

FIG. 5: Streamlines of the flow at Ra = 10^5 and Ha = 40 for θ = 0, 30, 45, 60, 90 and γ = 0, 30, 60, 90 for φ = 0 (solid lines) and φ = 6% (dashed lines)

field angles. It goes without saying that Cu nanoparticles show the highest enhancing influence on the Nusselt number, and TiO_2 nano-particles, having the lowest thermal conductivity, cannot increase the mean Nu significantly. The most interesting aspect of this figure is the minimum point on all of the graphs. With a more astute look at this figure and with regard to the previous discussion, these minimum points are based on an important cause. These points are representing the situations in which convection heat transfer is the dominant form of heat transfer, or at least the stream functions are stronger at these points so that the enhancing effect of nanoparticles, which act to improve the conduction

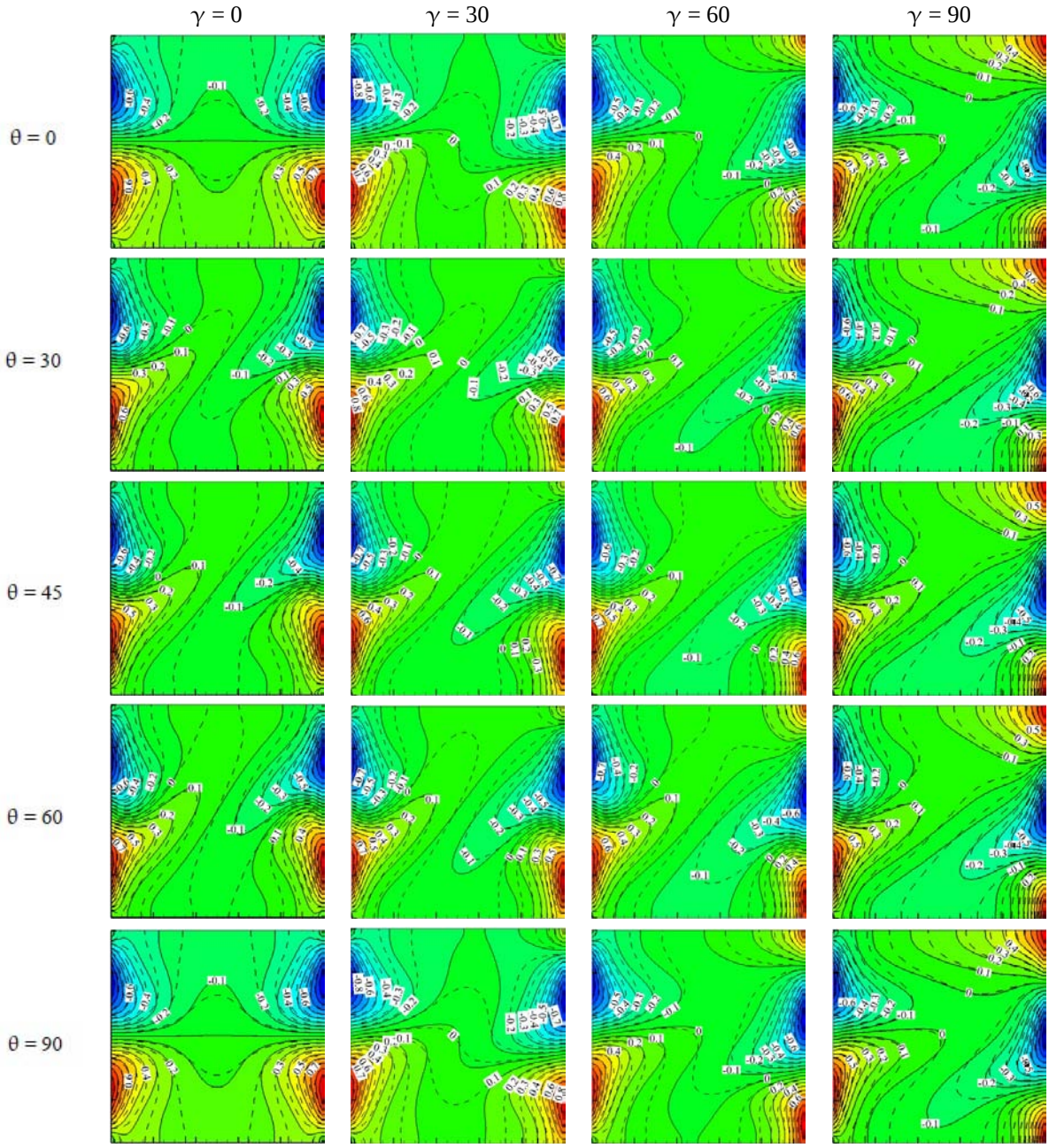

FIG. 6: Isotherms of the flow at Ra = 10^5 and Ha = 40 for θ = 0, 30, 45, 60, 90 and γ = 0, 30, 60, 90 for φ = 0 (solid lines) and φ = 6% (dashed lines)

heat transfer, cannot exert much influence. As can be seen, these minimum points are observed at around θ = 60. We will see later that at this angle almost for all cases, the main vortex is stronger and thus the flow circulation and Nusselt number are enhanced.

Figure 9 presents Nu^* for moderate Ra numbers of 10^4, 5×10^4, 10^5, in which the magnetic forces are strong and they can influence the fluid flow significantly, for two different magnetic situations of Ha = 0 and Ha = 40, θ = 60.

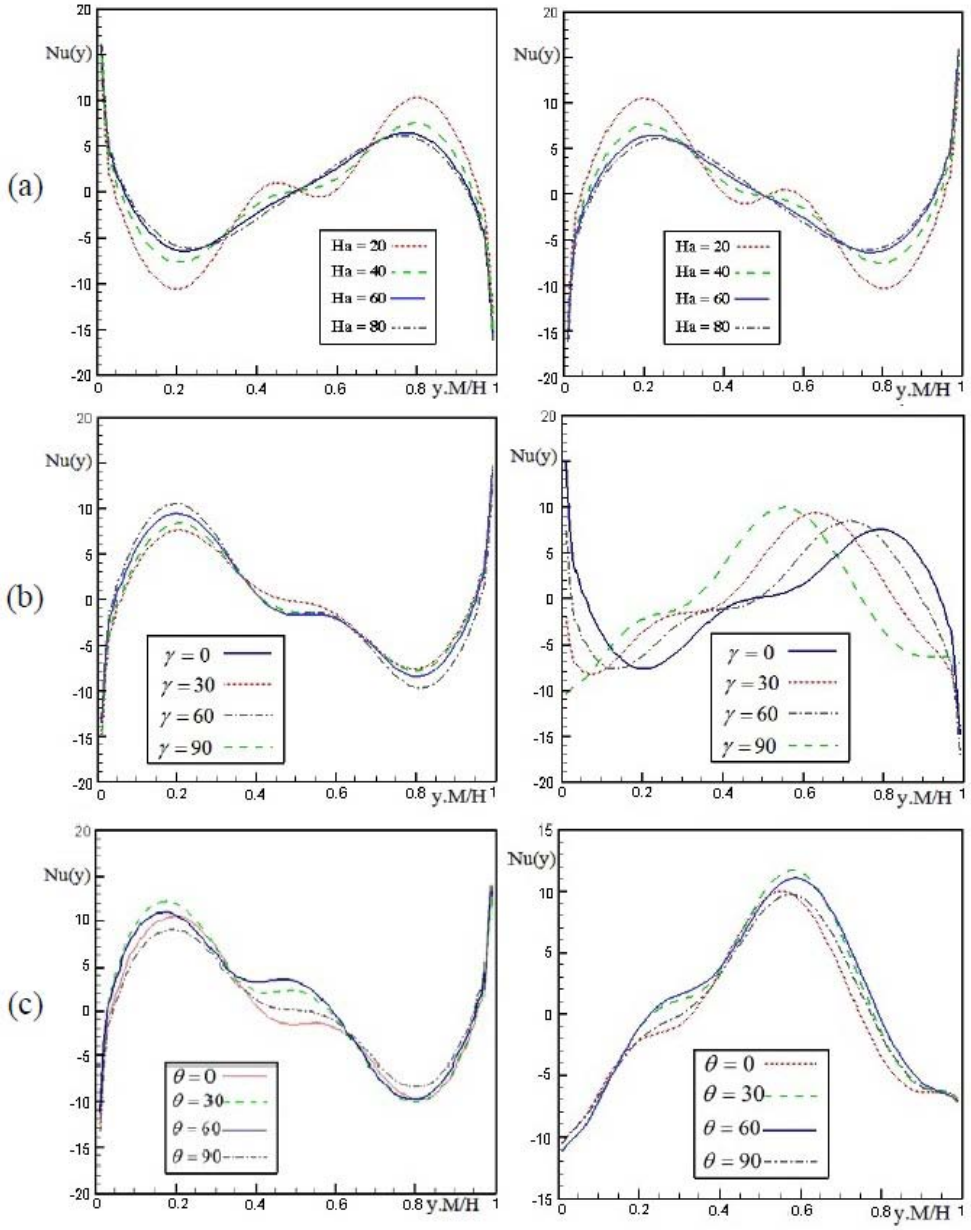

FIG. 7: Local Nusselt number on the west (up) and east (down) walls for **(a)** Ha = 20, 40, 60, 80; **(b)** γ = 0, 30, 60, 90; and **(c)** θ = 0, 30, 60, 90

In order to find a more comparative vision, the results of all three nanoparticle types are presented as well as their curve equations. It was mentioned before that the nanoparticles can affect the heat transfer in two ways. First they will change the density and viscosity of the base fluid and so they would lower the stream function value; hence the fluid velocity on the walls would decrease. As a result, the convective heat transfer rate would decrease. On the other hand, they can increase the thermal conductivity of the fluid so the conductive heat transfer is enhanced. The question is which of these two heat dissipation regimes is the dominant one? Obviously for low Ra numbers, the dominant heat

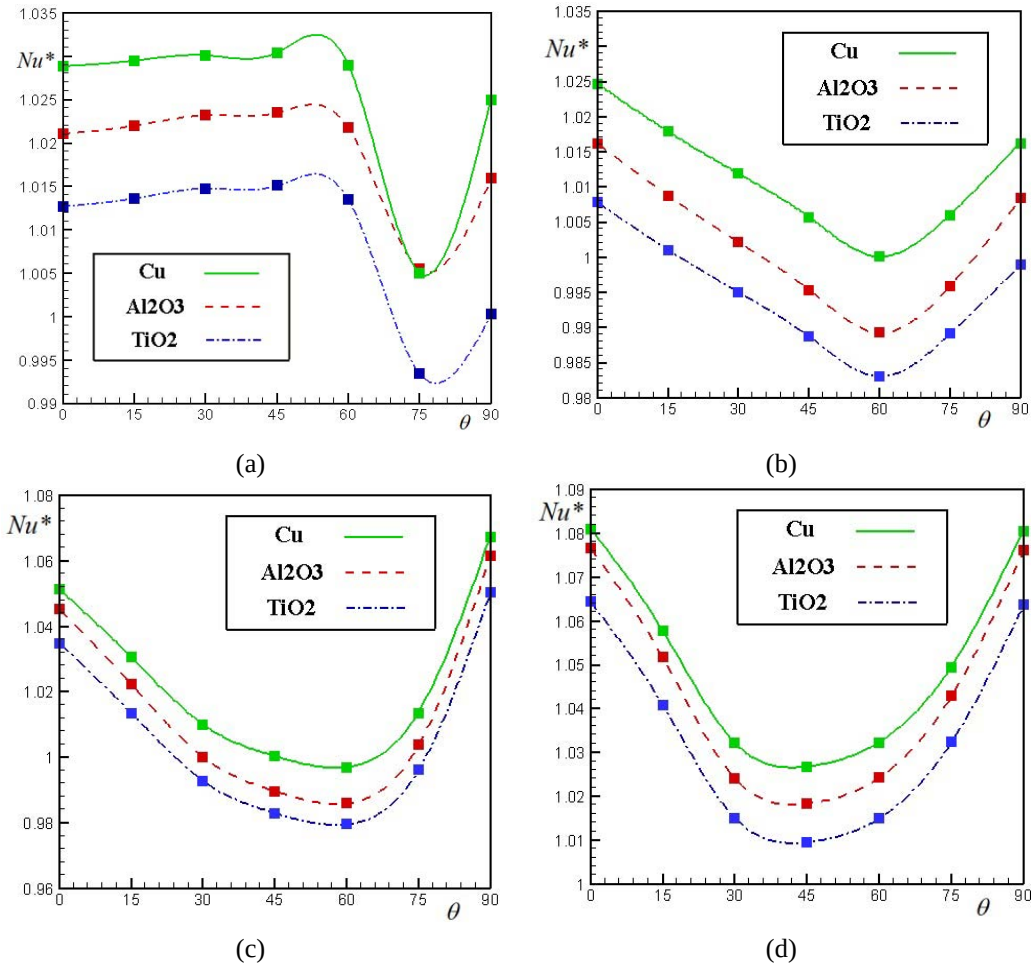

FIG. 8: The normalized Nu^* for Al_2O_3, Cu, and TiO_2 nanoparticles with φ = 3% at **(a)** Ha = 20, **(b)** Ha = 40, **(c)** Ha = 60, and **(d)** Ha = 80

transfer type is conduction and the enhancing effect of nanoparticles is maximized. Also, for Ra numbers higher than 10^5 we will have the convective heat transfer to be dominant. However, for the regions between them, the situation is quite shaky. This means that a slight change in the flow field or the magnetic field situation may collapse the whole idea of increasing the heat transfer rate by the addition of nanoparticles, and instead of an *increase* the nanoparticles would *decrease* the overall Nusselt number.

As can be seen for Ha = 0, we have an ever-ascending manner for Nu^* in all cases, but as the Ra increases the slopes of the Nusselt curves decrease slightly due to the reduction of the conduction dominancy. These slopes not only reveal the thermal conduction difference of the nano particle types, but they also shed light on their influence on the flow-field characteristics (stream function). The overall idea for this case is that adding the nano-particle volume fraction has its predicted enhancing effect. Now we will put this idea to the test under the influence of a magnetic field defined as Ha = 40, θ = 60. It is shown in Fig. 8 that despite an increase of Nu^* in Ra = 10^4, the slope of the curves would experience a severe decrease from Ra = 10^4 to Ra = 10^5. Not only the addition of nano-particles cannot improve Nu^*, but in Ra = 10^5, we also witness a reduction of Al_2O_3 and TiO_2 nano-particles.

Figure 10 presents the normalized Nusselt number with respect to the case of no-magnetic-field Nusselt number ($\widehat{Nu}$) versus the Ra number for various Ha numbers. This graph can totally explain the behavior of the magnetic field

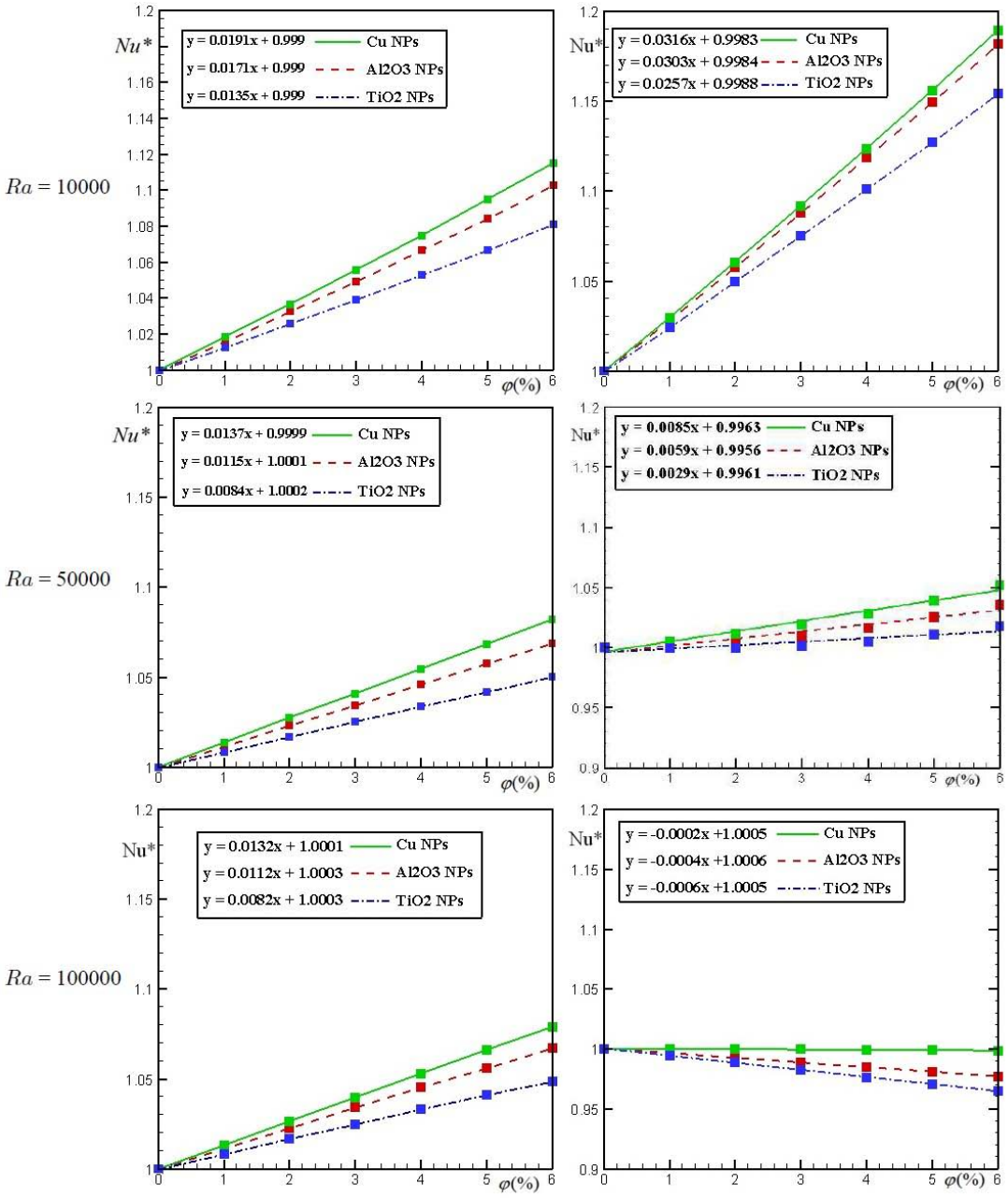

FIG. 9: Normalized nanofluid Nu with respect to the pure fluid Nu for moderate Ra numbers versus various particle volume fractions (φ) for the cases of Ha = 0 (up) and Ha = 40, θ = 60 (down)

and its effective regime regarding each Ra number. As can be seen, each curve experiences a descending manner with the increment of Ra number up to about Ra = 10^5, but at this point there would be a minimum point and afterward the graphs find an ascending manner. It is known that MHD forces by their nature [see Eqs. (5) and (6)] are depending on the flow velocities, so at lower Ra numbers their effects become insignificant. Hence, it is expected that with an increase in the Ra number, these magnetic forces gain power. On the other hand, when the Ra number is increased,

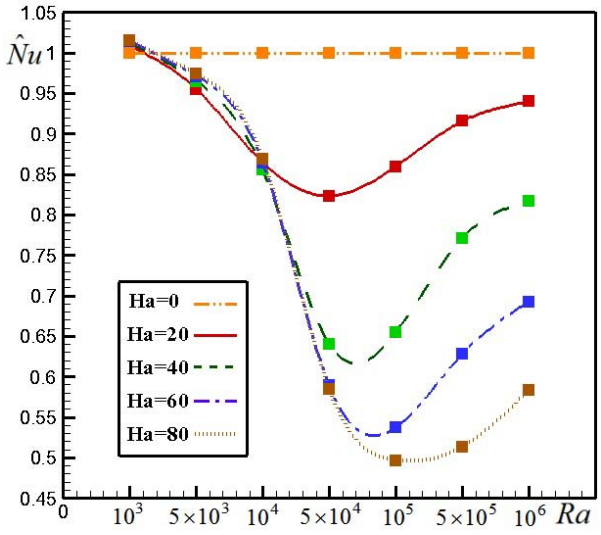

FIG. 10: The normalized Nu for $\gamma = \pi/2$, $\varphi = 0$, and $\theta = 0$ at Rayleigh numbers in the range of 10^3–10^6 for Ha = 0, 20, 40, 60, 80

the buoyant forces increase with higher order than the magnetic forces so again the MHD forces start to lose their significance at a specific Ra number. This point is the minimum point on the graph, which in some texts is referred to as the critical Ra number.

Also another interesting aspect of this figure is the increasing manner of $\widehat{Nu}$ with an increase in Ha number for lower Ra numbers. This rare phenomenon is also reported by other authors (Ahrar and Djavareshkian, 2016; Mejri et al., 2014). This feature usually is observed when the temperature boundary condition on the west and east walls have a phase deviation of $\gamma = \pi/2$ and the main heat transfer regime is conduction.

Figure 11 shows the evolution of ($\widehat{Nu}$) with magnetic field angle (θ) increment for different γ values and Hartmann numbers. It is expected that with an increase in Ha, the normalized Nusselt number should decrease. According to the mentioned figure, this idea is valid for all cases except for Ha = 20 and θ = 45, 60. In these angles, all of the graphs experience a maximum point (due to the better fluid circulations), but in Ha = 20, they get to exceed the no-magnetic-field line. According to Fig. 5, these directions are almost perpendicular to the streamlines of the main vortex, so instead of opposing they would find a proposing effect on this vortex (see Figs. 5 and 6; the main vortex is stronger around θ = 45). Hence the velocity components on the walls along with the heat transfer rate would increase. Note that in these magnetic field directions $\widehat{Nu}$ experiences a descending manner with the increment of γ. This phenomenon shows that with an increase in the phase deviation the magnetic field influence on the fluid would increase. Also, it should be noted that in θ = 0 and θ = 90 the magnetic field acts mostly to decelerate the fluid flow, so the minimum $\widehat{Nu}$ is observed at these points.

5. CONCLUSION

In the present study, the influence of magnetic field intensity and direction on a nanofluid-filled closed cavity with a sinusoidal temperature boundary condition was investigated numerically for various phase deviation angles. Three types of nanoparticles (Cu, Al_2O_3, and TiO_2) were chosen to explain their behavior under the influence of a magnetic field. The main findings of the numerical simulations are as follows:

1. Basically, the flow stream functions as well as the walls' Nu numbers were reduced with the magnetic field intensity augmentation.

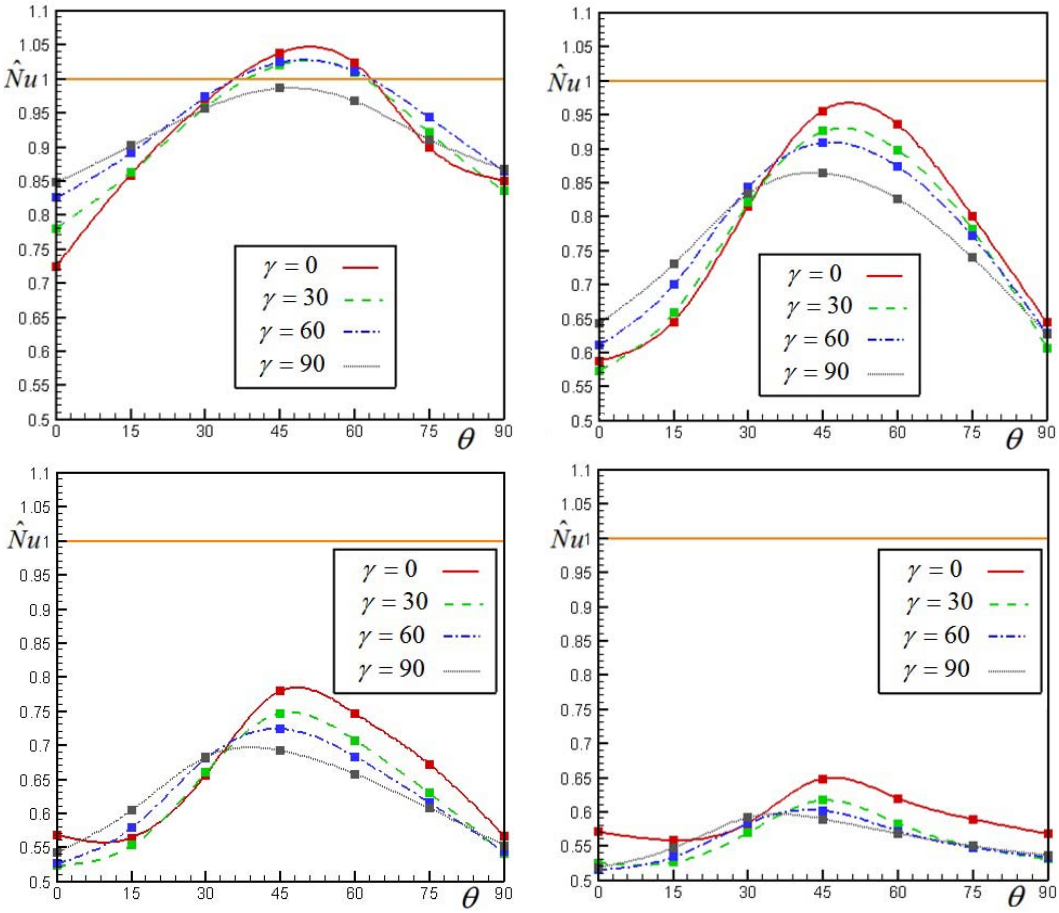

FIG. 11: Normalized Nusselt number with respect to the zero magnetic field (Nu) versus magnetic field angle (θ) for φ = 0 and γ = 0, 30, 60, 90 at **(a)** Ha = 20, **(b)** Ha = 40, **(c)** Ha = 60, and **(d)** Ha = 80

2. In a majority of Ra and Ha numbers, an increment in the phase deviation (γ) could lead to a mild increase inthe Nusselt number; however, the normalized Nusselt number $\widehat{Nu}$ has a different manner for various magnetic situations.

3. In some certain magnetic situations, such as Ra = 10^5, Ha = 40, and θ = 60°, the nanoparticle enhancing effect was quite insignificant and even sometimes they could decrease the overall Nu number.

4. The decreasing tendency in point 3 above was found to be more remarkable for Al_2O_3 (moderate thermal conductivity) and TiO_2 (low thermal conductivity) nanoparticles and *increases* with the augmentation of particle volume fraction.

5. The average Nu number is decreased with the Ha number augmentation for almost all Ra numbers, but the curves revealed a minimum point for each Ha number. This indicates that the magnetic field forces are most powerful and can affect the flow regime most significantly.

6. Also, the influence of magnetic field direction was observed and for certain magnetic field angles θ = 45, an increase in the normalized Nusselt number ($\widehat{Nu}$) was observed. This certain θ was found to be almost fixed for

every Ha and γ values so it can be referred to as an optimum field angle for the purpose of heat dissipation applications.

ACKNOWLEDGMENT

We wish to present our thanks to Ms. M. Ataeian for her assistance and dedication in the progression of this study.

REFERENCES

Abu-Mulaweh, H. I., A review of research on laminar mixed convection flow over backward- and forward-facing steps, *J. Solar Energy Eng.*, vol. **42**, no. 9, pp. 897–909, 2003.

Ahmed, H. E., Ahmed, M. I., and Yusoff, M. Z., Heat transfer enhancement in a triangular duct using compound nanofluids and turbulators, *Appl. Therm. Eng.*, vol. **91**, pp. 191–201, 2015.

Ahrar, A. J. and Djavareshkian, M. H., Numerical investigation of hydro-magnetic flow of air in a lid driven cavity for an optimum magnetic situation, *Int. J. Fluid Mech. Res.*, vol. **41**, no. 5, pp. 460–470, 2014.

Ahrar, A. J. and Djavareshkian, M. H., Lattice Boltzmann simulation of a Cu-water nanofluid filled cavity in order to investigate the influence of volume fraction and magnetic field specifications on flow and heat transfer, *J. Mol. Liq.*, vol. **215**, pp. 328–338, 2016.

Alchaar, S., Vasseur, P., and Bilgen, E., Natural convection heat transfer in a rectangular enclosure with a transverse magnetic field, *J. Heat Transfer*, vol. **117**, no. 3, pp. 668–673, 1995.

Al-Nimr, M. A., MHD free-convection flow in open-ended vertical concentric porous annuli, *Appl. Energy*, vol. **50**, pp. 293–311, 1995.

Al-Nimr, M. A. and Hader, M. A., MHD free convection flow in open-ended vertical porous channels, *Chem. Eng. Sci.*, vol. **54**, pp. 1883–1889, 1999.

Clausing, A. M., Convective losses from cavity solar receivers – Comparisons between analytical prediction and experimental results, *J. Solar Energy Eng.*, vol. **105**, no. 1, pp. 29–33, 1983.

Deng, Q. H. and Chang, J., Natural convection in a rectangular enclosure with sinusoidal temperature distributions on both sidewalls, *Numer. Heat Transfer, Part A*, vol. **54**, no. 5, pp. 507–524, 2008.

Gangawane, K. M., Bharti, R. P., and Kumar, S., Lattice Boltzmann analysis of natural convection in a partially heated open ended enclosure for different fluids, *J. Taiwan Inst. Chem. Eng.*, vol. **49**, pp. 27–39, 2015.

Ghasemi, B., Aminossadati, S. M., and Raisi, A., Magnetic field effect on natural convection in a nanofluid-filled square enclosure, *Int. J. Therm. Sci.*, vol. **50**, no. 9, pp. 1748–1756, 2011.

Hossain, M. A. and Rees, D. A. S., Natural convection flow of water near its density maximum in a rectangular enclose having isothermal walls with heat generation, *Heat. Mass. Transfer*, vol. **41**, no. 4, pp. 367–374, 2005.

Hussein, M., Mustafa, M. T., Jafaryarc, M., and Mohammadian, E., Nanofluid in tilted cavity with partially heated walls, *J. Molecular Mol. Liquids*, vol. **199**, pp. 545–551, 2014.

Ishikawa, M., Hirata, T., and Noda, S., Numerical simulation of natural convection with density inversion in a square cavity, *Numer. Heat Transfer, Part A*, vol. **37**, no. 4, pp. 395–406, 2000.

Jahanshahi, M., Hosseinizadeh, S. F., Alipanah, M., Dehghani, A., and Vakilinejad, G. R., Numerical simulation of free convection based on experimental measured conductivity in a square cavity using water/SiO_2 nanofluid, *Int. Commun. Heat Mass Transfer*, vol. **37**, no. 6, pp. 687–694, 2010.

Kandaswamy, P., Malliga Sundari, S., and Nithyadevi, N., Magneto convection in an enclosure with partially active vertical walls, *Int. J. Heat Mass Transfer*, vol. **51**, no. 7, pp. 1946–1954, 2008.

Kefayati, G. H. R., Natural convection of ferrofluid in a linearly heated cavity utilizing LBM, *J. Molecular Mol. Liquids*, vol. **191**, pp. 1–9, 2014.

Kefayati, G. H. R., Magnetic field effect on heat and mass transfer of mixed convection of shear-thinning fluids in a lid-driven enclosure with non-uniform boundary conditions, *J. Taiwan Inst. Chem. Eng.*, vol. **51**, pp. 20–33, 2015.

Kefayati, G. H. R., Gorji-Bandpy, M., Sajjadi, H., and Ganji, D. D., Lattice Boltzmann simulation of MHD mixed convection in a lid-driven square cavity with linearly heated wall, *Sci. Iran.*, vol. **19**, no. 4, pp. 1053–1065, 2012.

Khanafer, Kh., Vafai, K., and Lightstone, M., Buoyancy-driven heat transfer enhancement in a two-dimensional enclosure utilizing nanofluids, *Int. J. Heat Mass Transfer*, vol. **46**, no. 19, pp. 3639–3653, 2003.

Mahmoudi, A., Mejri, I., Abbassi, M. A., and Omri, A., Lattice Boltzmann simulation of MHD natural convection in a nanofluid-filled cavity with linear temperature distribution, *Powder Technol.*, vol. **256**, pp. 257–271, 2014.

Mejri, I., Mahmoudi, A., Abbassi , M. A., and Omri, A., Lattice Boltzmann simulation of MHD natural convection in a nanofluid-filled enclosure with non-uniform heating on both side walls, *Int. J. Math. Comput. Phys. Quantum Eng.*, vol. **8**, no. 1, pp. 75–91, 2014.

Minakov, A. V., Lobasov, A. S., Guzei, D. V., Pryazhnikov, M. I., and YaRudyak, V., The experimental and theoretical study of laminar forced convection of nanofluids in the round channel, *Appl. Therm. Eng.*, vol. **88**, pp. 140–148, 2015.

Nemati, H., Farhadi, M., Sedighi, K., Ashorynejad, H. R., and Fattahi, E., Magnetic field effects on natural convection flow of nanofluid in a rectangular cavity using the lattice Boltzmann model, *Sci. Iran., Trans. B*, vol. **19**, no. 2, pp. 303–310, 2012.

Ozoe, H. and Okada, K., The effect of the direction of the external magnetic field on the three-dimensional natural convection in a cubical enclosure, *Int. J. Heat Mass Transfer*, vol. **32**, no. 10, pp. 1939–1954, 1989.

Oztop, H. F., Al-Salem, Kh., and Pop, I., MHD mixed convection in a lid-driven cavity with corner heater, *Int. J. Heat Mass Transfer*, vol. **54**, no. 15-16, pp. 3494–3504, 2011.

Shahrul, I. M., Mahbubul, I. M., Khaleduzzaman, S. S., Saidur, R., and Sabri, M. F. M., A comparative review on the specific heat of nanofluids for energy perspective, *Renewable Sustainable Energy Rev.*, vol. **38**, pp. 88–98, 2014.

Sheikholeslami, M., Gorji-Bandpy, M., Ganji, D. D., Soleimani, S., and Seyyedi, M., Natural convection of nanofluids in an enclosure between a circular and a sinusoidal cylinder in the presence of magnetic field, *Int. Commun. Heat Mass Transfer*, vol. **39**, no. 9, pp. 1435–1443, 2012.

Sivasankaran, S., Malleswaran, A., Lee, J., and Sunder, P., Hydro-magnetic combined convection in a lid driven cavity with sinusoidal boundary conditions on both side walls, *Int. J. Heat Mass Transfer*, vol. **54**, no. 1-3, pp. 512–525, 2011.

Wu, F., Zhou, W., and Ma, X., Natural convection in a porous rectangular enclosure with sinusoidal temperature distributions on both side walls using a thermal non-equilibrium model, *Int. J. Heat Mass Transfer*, vol. **85**, pp. 756–777, 2015.